Kinetics and Mechanism of Dimethyl Ether Oxidation to Formaldehyde on Supported Molybdenum Oxide Domains

Patricia Cheung, Haichao Liu, and Enrique Iglesia*

Department of Chemical Engineering, University of California at Berkeley, Berkeley, California 94720

Received: May 25, 2004; In Final Form: August 17, 2004

Kinetic isotope effect and isotopic tracer/exchange methods were combined with in situ infrared spectroscopy and kinetic data to determine the mechanism of dimethyl ether (DME, CH_3OCH_3) oxidation to formaldehyde (HCHO) on MoO_x/Al_2O_3. The reaction intermediates and elementary steps established a redox mechanism that led to kinetic rate equations that are consistent with observed dependencies of reactant pressures. Methoxide concentrations as detected by in situ infrared spectroscopy correlated directly with formation rates to establish their importance for the formation of HCHO and CH_3OH. Reactant partial pressure studies showed that rates of HCHO and CH_3OH formation are first-order in DME and zero-order in O_2 at low DME pressures. At high DME pressures, rates became independent of DME pressure and acquired positive-order O_2 dependencies. H−D kinetic isotope effects indicated that C−H bond activation is not involved in kinetically relevant steps and transient studies involving $CH_3{}^{16}OCH_3-{}^{18}O_2-Mo^{16}O_x/Al_2O_3$ confirmed the kinetic relevance of DME dissociative adsorption, the step that precedes C−H bond activation. These studies also indicated that mechanisms for HCHO formation do not discriminate between methoxide species formed from DME oxygen and those formed from lattice oxygen. Transient studies with $CH_3{}^{16}OCH_3-{}^{16}O_2-{}^{18}O_2-Mo^{16}O_x/Al_2O_3$ did not lead to detectable $^{16}O-{}^{18}O$ levels, indicating that vacancy reoxidation is irreversible.

1. Introduction

Kinetic and thermodynamic hurdles render current processes for direct methane conversion routes to alkenes and oxygenates too costly for practical implementation. Oxygenates, such as formaldehyde (HCHO), methyl formate (MF), and acetic acid are currently produced via indirect routes involving synthesis gas and methanol as intermediates. Recent advances in shape-selective acid-catalyzed methanol conversion to light alkenes are likely to expand the use of methanol as an intermediate in ethene and propene synthesis processes.[1−5] Dimethyl ether (DME, CH_3OCH_3) is an attractive alternate feedstock in each of these processes because its synthesis provides economic and thermodynamic advantages over CH_3OH synthesis.[6,7]

MoO_x and VO_x domains dispersed on ZrO_2, SnO_2, and Al_2O_3 supports, and on Al_2O_3 surfaces modified by monolayers of SnO_2, CeO_2, or Fe_2O_3, catalyze DME oxidation to HCHO with high reaction rates and primary HCHO selectivities (80−98%, CH_3OH-free basis)[8−11] at temperatures (∼500 K) much lower than previously reported.[12−14] These recent studies have shown that DME oxidation proceeds via parallel and sequential pathways (Scheme 1), which include primary steps leading to HCHO, CH_3OH, MF, and CO_x and secondary reactions of HCHO to form both MF and CO_x.[9,10] The structure and size of active MoO_x domains and the chemical identity of the support used to disperse these domains influence catalytic rates, because the ability of active oxide structures to delocalize charge, a process required to stabilize activated complexes involved in kinetically relevant elementary steps for many oxidation reactions,[9,10] depends on domain size and on the identity of the support. The Lewis acidity of cations in active oxides and support surfaces control the binding and desorption rates of HCHO and the stability of adsorbed dioxymethylene and formate intermediates involved in MF and CO_x formation.[9]

SCHEME 1: Primary and Secondary Pathways in DME Oxidation

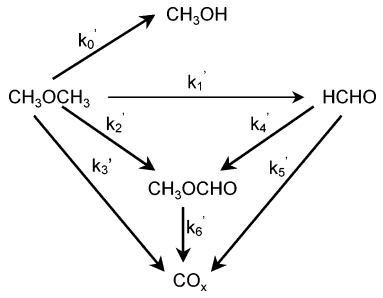

Here, we report the results of a mechanistic study of DME oxidation to HCHO on MoO_3 domains. The results indicate that the reaction occurs via redox cycles involving intermediates and elementary steps consistent with the observed kinetic influence of DME and O_2 pressures on oxidation rates and with independent spectroscopic and isotopic data. A highly selective MoO_x/Al_2O_3 catalyst, containing about one theoretical polymolybdate monolayer (7 Mo/nm^2, 15.6 wt % MoO_3/Al_2O_3), was chosen in an effort to focus the study on HCHO synthesis pathways with minimal contributions from secondary oxidation reactions. Primary HCHO selectivities increased with increasing MoO_x loadings on Al_2O_3 and reached maximum values (∼98%)

* To whom correspondence should be addressed. E-mail: iglesia@cchem.berkeley.edu. Telephone: (510) 642-9673. Fax: (510) 642-4778.

10.1021/jp0477405 CCC: $27.50
Published on Web 11/06/2004

at these Mo surface densities (~7 Mo/nm^2).[9] The polymolybdate structures prevalent at these surface densities also led to nearly complete coverage of Al_2O_3 surfaces, thus minimizing acid-catalyzed hydration reactions of DME to form CH_3OH.

2. Experimental Methods

2.1. Catalyst Synthesis and Characterization. MoO_x/Al_2O_3 catalysts were prepared by incipient wetness impregnation of γ-Al_2O_3 (Degussa AG, 100 m^2/g) with a solution of ammonium heptamolybdate (99% Aldrich).[15] The samples were dried overnight in ambient air at 393 K and treated in dry air (Airgas, zero grade) at 773 K for 3 h. Mo surface densities are reported as Mo/nm^2, based on the nominal Mo content and the BET surface area after thermal treatment. Surface areas were measured using a five-point BET method and N_2 physisorption at its normal boiling point using an Autosorb-1 unit (Quantachrome Corp).

2.2. In Situ Infrared Spectroscopy. Infrared spectra were collected in transmission mode with 2 cm^{-1} resolution using a Mattson Research Series 1000 spectrometer. Samples (15 mg) were pressed into thin self-supporting wafers and placed within a flow cell with CaF_2 windows and a short optical path. Samples were treated within this cell using 0.67 cm^3/s dry air (Airgas, zero grade) at 773 K for 1 h and then cooled to 513 K before exposure to reactants. Reactants consisted of dimethyl ether (99.5%, Praxair), dioxygen (90% O_2/balance N_2, Praxair certified mixture), and He (99.999%, Airgas), used as an inert component to achieve desired total pressures (100 kPa) and flow rates (0.67 cm^3/s). Infrared spectra were collected after contact with reactants for 1 h. Infrared band intensities for gas-phase DME molecules were subtracted from each spectrum to obtain intensities for adsorbed species as a function of the contacting DME partial pressure.

2.3. Steady-State Catalytic Dimethyl Ether Oxidation Reactions on MoO_x/Al_2O_3. Steady-state rates and selectivities were measured in a packed-bed flow reactor with plug-flow hydrodynamics. Samples (0.1−0.3 g, 125−250 μm) were diluted with quartz particles (0.5−1 g, 125−250 μm) to prevent temperature gradients and to avoid bypassing. The reactor consisted of a stainless steel tube (7.8 mm inner diameter) equipped with a multipoint thermocouple held within a 3.4 mm thermowell aligned along the tube center. Electronic mass flow controllers (Porter Instruments) were used to meter individual reactant streams.

Samples were treated in 0.1 cm^3/s 90% O_2/10% N_2 (Praxair certified mixture) diluted with 0.4 cm^3/s He (Airgas, UHP) at 773 K for 1 h and then cooled to 513 K before catalytic measurements. The kinetic effects of DME and O_2 pressures were measured at 513 K and 100−270 kPa total pressures over a wide range of space velocity and DME and O_2 concentrations. Reactant mixtures contained DME (99.5%, Praxair), dioxygen (90% O_2/balance N_2, Praxair certified mixture), and He (99.999%, Airgas) as balance. Heat-traced lines (393−423 K) were used to transfer the effluent to an Agilent 6890 gas chromatograph equipped with a methyl silicone capillary column (HP-1, 50 m × 0.32 mm × 1.05 μm) connected to a flame ionization detector (FID) and a Porapak Q packed column (80−100 mesh, 12 ft. × $^1/_8$ in.) connected to a thermal conductivity detector (TCD). CH_3OCH_3 (Matheson, 99.5%) and CD_3OCD_3 (Aldrich, 98 atom % D) were reacted separately with oxygen (90% O_2/balance N_2, Praxair certified mixture), and He (UHP, Airgas) as balance, to measure H−D kinetic isotope effects for DME conversion reactions. An empty reactor did not form detectable amounts of products at temperatures below 590 K.

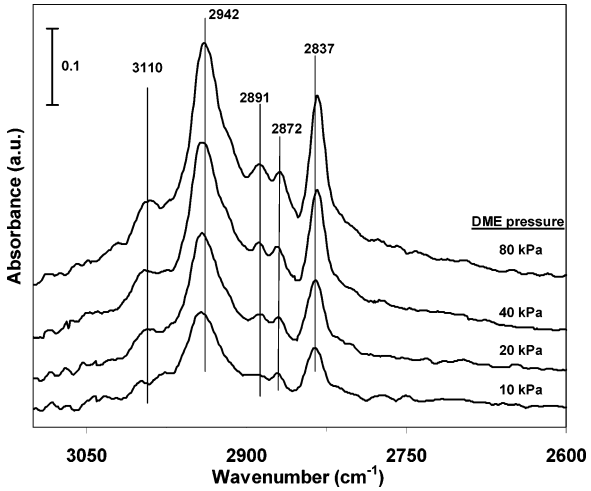

Figure 1. In situ infrared spectra at various DME pressures on 15.6 wt % MoO_3/Al_2O_3 (7 Mo/nm^2) [18 kPa O_2, balance He, 513 K].

2.4. Isotopic Exchange and Tracer Experiments. A gradientless recirculating batch reactor made of glass was used for isotopic tracer and exchange studies. This approach leads to product evolution profiles with contact time that rigorously reflect those in flow reactors with varying residence time.[16] The entire system was enclosed in Al foil and heated to ~323 K using an ambient air heater to inhibit HCHO oligomerization and condensation. Reactants and products were circulated over catalyst samples (0.01−0.03 g) at 3.33 cm^3/s using a graphite gear micropump. Chemical and isotopic compositions of reactants and products were measured periodically by syringe injection of 1 cm^3 gas samples into a gas chromatograph (Agilent 6890) equipped with a mass selective detector (Agilent 5973). Ion yields were analyzed using deconvolution methods that account for natural ^{13}C abundance and for fragmentation patterns to obtain isotopomer distributions for each reactant and product.[17] Rates and selectivities were simultaneously measured by injection of 1 cm^3 samples into the Agilent 6890 gas chromatograph used for flow reactor measurements.

Catalyst samples were treated in 5% O_2/3% Ar/He (Scott Specialty Gases, certified master class) at 773 K for 1 h before reaction. $CH_3{}^{16}OCH_3$, 5% $^{16}O_2$/3% Ar/He, 5% $^{18}O_2$/2% Ar/He (Isotec, 99 atom % ^{18}O) and He (UHP, Airgas; balance to give 110 kPa total pressure) were used as reactants in isotopic experiments. Isotopic and chemical compositions were measured at 513 K on $Mo^{16}O_x/Al_2O_3$ to probe the reversibility of dissociative O_2 chemisorption steps. $CH_3{}^{16}OCH_3$, $^{18}O_2$ (Isotec, 99 atom % ^{18}O), and He (UHP, Airgas) as balance were reacted on $Mo^{16}O_x/Al_2O_3$ at 488 K to probe the involvement of lattice oxygen atoms in redox cycles and the reversibility of DME dissociation steps.

3. Results and Discussion

3.1. In Situ Infrared Spectroscopy Evidence for Adsorbed Methoxide Intermediates. Figure 1 shows infrared spectra in the C−H stretching region during steady-state DME oxidation at 10−80 kPa DME and 513 K. Weak infrared bands at 2891 and 2872 cm^{-1} are assigned to C−H stretches in physisorbed DME; stronger absorption bands at 3110, 2942, and 2837 cm^{-1} arise from C−H stretches in adsorbed methoxide species. These infrared bands were assigned by reference to previous methanol adsorption studies on MoO_3 and V_2O_5.[18−23] Briand et al.,[18] Burcham et al.,[19] and Seman et al.[24] found that methoxide

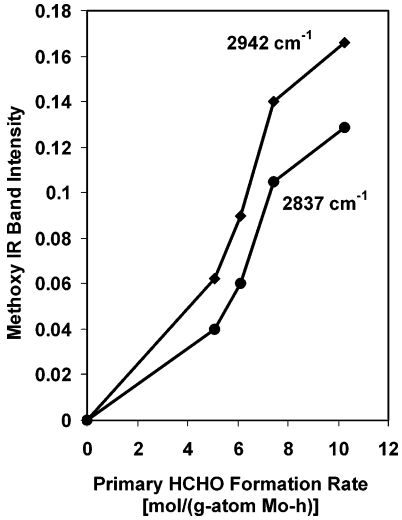

Figure 2. HCHO formation rates plotted vs methoxy FTIR band intensity during DME oxidation on 15.6 wt % MoO_3/Al_2O_3 (7 Mo/nm^2) [18 kPa O_2, balance He, 513 K].

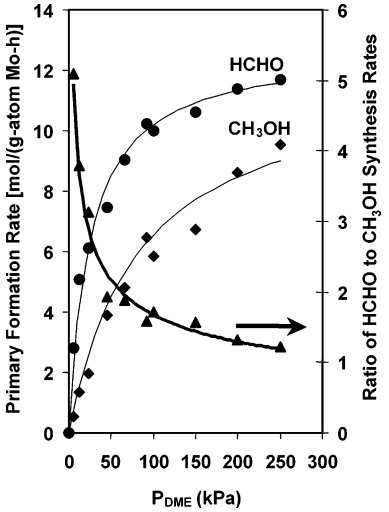

Figure 3. Effect of DME concentration on formaldehyde and methanol synthesis rates on 15.6 wt % MoO_3/Al_2O_3 (7 Mo/nm^2) [18 kPa O_2, balance He, 513 K].

species are present on oxide surfaces during adsorption of CH_3OH above 373 K, and that physisorbed methanol coexists with methoxide species at lower temperatures. DME molecules hydrogen-bonded to silanol and acidic OH groups on HZSM-5 dissociate to form methoxide species identical to those formed from CH_3OH above 473 K.[20]

The intensity of these methoxide bands increased with increasing DME pressure (Figure 1) during catalytic oxidation reactions. Thus, active sites are not yet covered with adsorbed methoxide species at these DME concentrations. These studies indicate that physisorption and dissociation of O−H bonds in CH_3OH and of C−O bonds in DME to form methoxide species occur at typical catalytic oxidation temperatures. Only very weak signals were detected in the C═O and O−H regions, indicating that the observed C−H stretches did not arise from molecularly adsorbed HCHO or CH_3OH.

Methoxide species and physisorbed DME exist on the catalyst surface during DME oxidation and methoxide groups appear to be the reactive intermediates in HCHO synthesis from DME. This intermediate role of methoxide species is consistent with the data shown in Figure 2, which show that DME conversion rates and the intensities of the methoxide bands at 2837 and 2942 cm^{-1} in Figure 1 increase in parallel with increasing DME pressures (10−80 kPa). These data suggest the direct involvement of methoxide species in DME oxidation.

3.2. Effects of Reactant Concentrations on Primary HCHO and CH_3OH Formation Rates. Figure 3 shows the effects of DME partial pressure on primary HCHO and CH_3OH formation rates at 513 K and 100−270 kPa total pressures. Primary rates were obtained by extrapolating measured rates to zero reactant residence time for each reactant concentration. HCHO and CH_3OH rates increased with DME pressure at low pressures and then approached nearly constant values above 150 kPa, as active surfaces became populated with methoxide and methoxide-derived species (hydroxyl groups, vacancies).

The ratio of HCHO to CH_3OH formation rates decreased with increasing DME pressure and approached a value of unity, consistent with the stoichiometry for

$$CH_3OCH_3 + {}^1/_2O_2 \rightarrow CH_3OH + HCHO \qquad (1)$$

a reaction in which lattice oxygens are used stoichiometrically (and ultimately vacancies are replenished by O_2) to form CH_3OH, instead of H_2O, which typically forms in methanol oxidation reactions via OH recombination. CH_3OH is likely to form by reactions of OH groups, formed during H-abstraction from methoxide species, with other methoxides, in a step also required for DME hydration to CH_3OH, which occurs concurrently during DME oxidation as H_2O product concentration increases with increasing residence time. This equimolar formation of CH_3OH and HCHO becomes less likely as methoxide concentrations decrease and OH groups react with each other instead to form H_2O, to give the stoichiometry for oxidative dehydrogenation:

$$CH_3OCH_3 + O_2 \rightarrow 2HCHO + H_2O \qquad (2)$$

At low DME pressures and low adsorbed methoxide concentrations, routes to HCHO are favored over those leading to CH_3OH because hydroxyl groups tend to recombine and desorb as H_2O before reacting with adsorbed methoxide species.[25] As active sites become populated with adsorbed methoxide, OH recombination occurs less frequently, and CH_3OH formation becomes the dominant hydroxyl-rejection pathway. Indeed, the ratio of HCHO to CH_3OH in products decreased to values near unity as DME pressure increased and OH groups are removed only via reactions with methoxide. This stoichiometry indicates that HCHO essentially free of water can be formed, at least at low conversion, via the oxidation of DME at high pressures. This result, together with the fact that the stoichiometry for DME oxidation leads to half the amount of water formed in CH_3OH oxidation processes in commercial practice, may lead to higher HCHO purities and lower water removal costs.

The effects of O_2 partial pressure (5−75 kPa) on HCHO formation rates are shown in Figure 4 at two DME pressures (20 and 150 kPa). At 20 kPa DME, HCHO formation rates are nearly zero-order in O_2 pressure and increase linearly with DME pressure (Figures 3 and 4). In contrast, at DME pressures giving near zero-order DME effects on reaction rates (150 kPa), HCHO formation rates acquire a positive-order dependence on O_2 concentration and then become nearly independent of O_2 at higher O_2 partial pressures. These kinetic responses are reminiscent of catalytic reactions involving Mars−van Krevelen[26] redox cycles on reducible oxides with labile lattice oxygens, such as those involved in CH_3OH oxidation to HCHO[27] and oxidative dehydrogenation of alkanes.[28−30] Thus, we suggest below a similar type of redox mechanism for DME oxidation

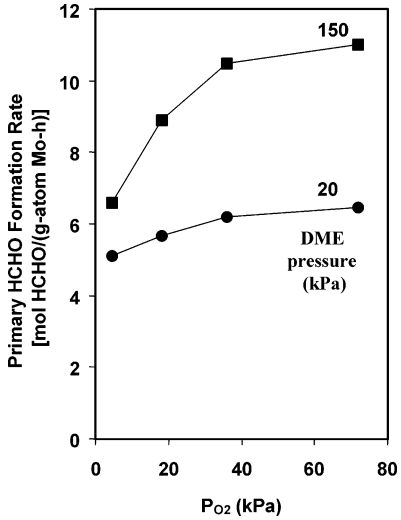

Figure 4. Effect of O_2 concentration on formaldehyde synthesis rates on 15.6 wt % MoO_3/Al_2O_3 (7 Mo/nm^2) [balance He, 513 K].

SCHEME 2: Reactive Intermediates

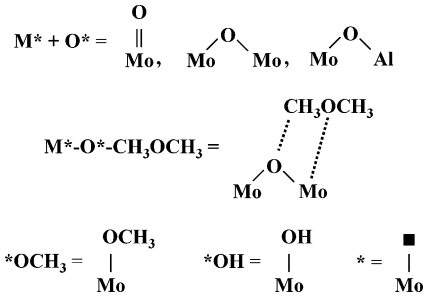

and provide isotopic evidence for the kinetic relevance and reversibility of specific steps and for the role of lattice oxygen atoms in DME oxidation.

The scheme below shows a plausible sequence of elementary steps, although as in most mechanistic proposals, not the only possible one. In this scheme, O* and M* represent a lattice oxygen and a metal center connected to a lattice oxygen (Mo−O, or Mo═O), respectively. *OCH_3 corresponds to methoxide intermediates and *OH and * represent hydroxyl groups and lattice oxygen vacancies, respectively. We note that the kinetic analysis described below is identical whether the bridging M−O−M or terminal M═O bonds are involved in C−O or C−H activation. Thus, a kinetic treatment by itself cannot provide information about the specific sites involved in elementary steps. Schematic depictions of the reactive intermediates are shown in Scheme 2.

1. Quasi-equilibrated nondissociative DME chemisorption.

$$CH_3OCH_3 + M^* + O^* \overset{K_1}{\leftrightarrow} M^*{-}O^*{-}CH_3OCH_3$$

2. Irreversible DME dissociation via concerted interactions with lattice oxygen and metal center to form two OCH_3 intermediates.

$$M^*{-}O^*{-}CH_3OCH_3 \xrightarrow{k_2} {}^*OCH_3 + {}^*OCH_3$$

3. Irreversible hydrogen abstraction from *OCH_3 using neighboring oxygen atom to form HCHO, *OH, and a reduced Mo cation.

$$^*OCH_3 + O^* \xrightarrow{k_3} * + {}^*OH + HCHO$$

4. Reversible reaction of *OCH_3 and *OH groups to form methanol.

$$^*OCH_3 + {}^*OH \underset{k_{-4}}{\overset{k_4}{\leftrightarrow}} M^* + O^* + CH_3OH$$

5. Reversible reaction of two *OH groups to form water.

$$^*OH + {}^*OH \underset{k_{-5}}{\overset{k_5}{\leftrightarrow}} M^* + O^* + H_2O$$

6. Irreversible reoxidation of reduced Mo centers via dissociative chemisorption of O_2.

$$* + * + O_2 \xrightarrow{k_6} O^* + O^*$$

Methoxide groups can either react with lattice oxygen to form HCHO or they can react with surface hydroxyl groups formed during C−H bond activation steps to form methanol. The overall reaction stoichiometry is

$$CH_3OCH_3 + \left(1 - \frac{\alpha}{2}\right)O_2 \rightarrow (2-\alpha)HCHO + \alpha CH_3OH + (1-\alpha)H_2O \quad (3)$$

where

$$\alpha = \frac{r_{CH_3OH}}{r_{HCHO}} = \frac{k_4[^*OH]}{k_3[O^*]}$$
$$0 \le \alpha \le 1 \quad (4)$$

In our derivation, we assume that equilibrium for the methanol formation step lies to the right (k_4[*OCH_3][OH*] ≫ k_{-4}[M*][O*]P_{CH_3OH}), because methanol conversion to products at our low DME conversion levels (0−10%) was undetected in our space velocity studies. Values of α range between 0 (when OH recombination leads to H_2O at low DME pressures) and 1 (for methoxide−OH recombination to form CH_3OH at high DME pressures).

Pseudo-steady-state analysis of M*, O*, *OCH_3, *OH, and * with the stated quasi-equilibrium assumptions do not give simple analytical closed-form solutions. As a result, we derive instead rate equations for asymptotic cases in which surfaces are essentially uncovered (low DME pressure) and in which the surface becomes populated with intermediates (high DME pressure). The full derivation is given in the Appendix.

At low DME pressures, methanol is not formed (step 4 is negligible). The rate of HCHO formation becomes

$$r_{HCHO} = \frac{1}{4}K_1k_2P_{DME} = k_{eff,1}P_{DME} \quad (5)$$

At high DME pressure, the rates of HCHO and methanol formation become equal and water is not formed (step 5 is negligible). We will provide experimental evidence in the next section to show that methoxide and hydroxyl surface concentrations are small throughout our kinetic and isotopic studies; they do not become abundant surface intermediates. Additionally, as DME pressures increase relative to O_2 pressures, the concentration of oxygen vacancies increases. When oxygen is limited, lattice oxygen vacancies become abundant and the rate of HCHO synthesis approaches

$$r_{HCHO} = \frac{1}{2}k_6P_{O_2} = k_{eff,2}P_{O_2} \quad (6)$$

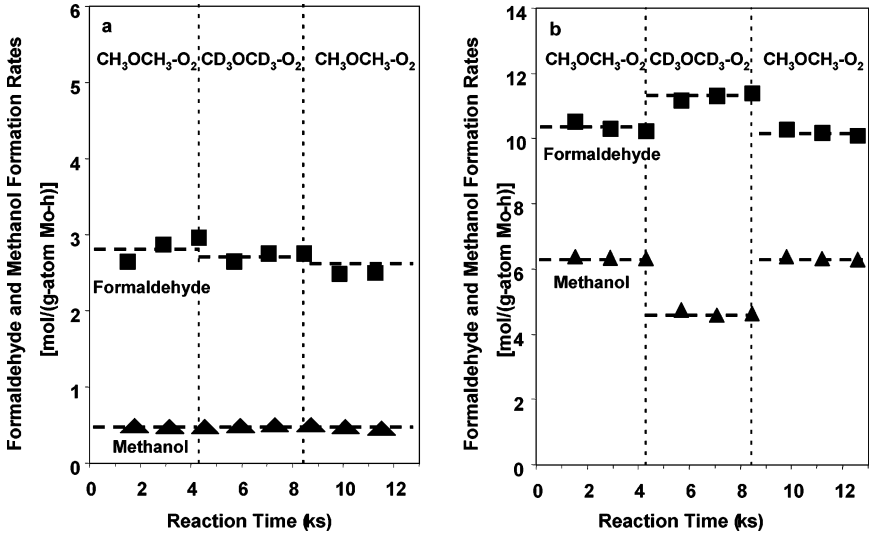

Figure 5. Formaldehyde and methanol kinetic isotope effects at 5 kPa (a) and 150 kPa (b) DME (18−20 kPa O_2, 513 K).

TABLE 1: Kinetic Isotope Effects on 15.6 wt % MoO_3/Al_2O_3 (7 Mo/nm^2) at 513 K

		KIE (r_H/r_d)		
P_{DME} (kPa)	P_{O_2} (kPa)	formaldehyde	methanol	DME
5.0	19.8	1.0	1.0	1.0
53.3	24.2	1.1	1.0	1.1
80.0	24.2	1.1	1.2	1.1
150.0	18.0	0.9	1.4	1.0

3.3. CH_3OCH_3−CD_3OCD_3 Kinetic Isotope Effects. Kinetic isotope effects were measured from primary formaldehyde and methanol synthesis rates and DME conversion rates with CH_3OCH_3−O_2 and CD_3OCD_3−O_2 reactant mixtures at various DME pressures (5−150 kPa) and 513 K. Figure 5 shows formaldehyde and methanol synthesis rates at 5 and 150 kPa DME. The corresponding kinetic isotope effects are shown in Table 1. At 5 kPa DME pressures, no significant kinetic isotope effects were detected for either formaldehyde or methanol synthesis. At 150 kPa, a small normal kinetic isotope effect (1.4) was measured for methanol synthesis, while formaldehyde synthesis showed a small inverse kinetic isotope effect (0.9). The formaldehyde and methanol KIE values combine to give overall kinetic isotope effects near unity for total DME conversion rates at all pressures tested. These small kinetic isotope effects are inconsistent with any kinetic relevance of steps involving hydrogen abstraction; they suggest instead that kinetically relevant elementary steps throughout the entire DME pressure range do not require the formation or cleavage of bonds containing hydrogen atoms.

The observed formaldehyde and methanol isotope effects at 150 kPa DME, although not large in comparison to those measured in methanol oxidation (as described below), are worthy of discussion. The mechanism branches under reaction conditions that lead to both formaldehyde and methanol formation. Here, the individual KIE values arise from H−D-influenced formaldehyde and methanol selectivities. Thus, there may now be an equilibrium isotope effect that reflects the relative stabilities of OH and OD. Formaldehyde formation is favored if the oxygen lattice readily accepts protons to form hydroxyl groups. Conversely, if hydroxyl groups are relatively unstable, they tend to combine with methoxides to generate methanol. Our results indicate that the latter occurs as larger methanol and smaller formaldehyde formation rates arise when the reactant is switched from protonated to deuterated DME.

In addition, since neither HCHO nor CH_3OH isotope effects become substantial, neither methoxide nor hydroxyl groups become the most abundant reactive intermediates over the range of DME and O_2 pressures tested. If either intermediate became a significant contributor to the pool of reactive species, the rate constants for C−H or O−H activation in HCHO (step 3), CH_3OH (step 4), and/or H_2O (step 5) formation steps would appear in the overall HCHO formation rate equation and measured rates would exhibit kinetic isotope effects much stronger than those measured.

Previous studies have reported kinetic isotope effects of 3−4 for oxidative dehydrogenation of methanol on MoO_3 and iron molybdate catalysts at 473−608 K, as expected from C−H bond activation in methoxide species as the kinetically relevant step in HCHO synthesis.[31] Our scheme for DME oxidation also involves methoxide intermediates, but we conclude based on measured KIE values that kinetically relevant steps in DME oxidation must involve the formation of methoxide intermediates (at low DME pressures) and the reoxidation of vacancy intermediates (at high DME pressures), neither of which involves reactions of chemical bonds containing hydrogen atoms. Thus, we suggest that the first-order rate constant, $k_{eff,1}$, for DME oxidation at low pressures reflects those for DME dissociation steps (step 2) on nearly uncovered surfaces (M* and O* as most abundant reactive intermediates); this conclusion is confirmed by the isotopic tracer and exchange measurements described below. The positive-order dependence on O_2 pressure at high DME pressures indicates that reoxidation of reduced centers becomes kinetically relevant when surface vacancies become the most abundant reactive intermediates; the rate of this step does not depend on whether protium or deuterium are present in dimethyl ether reactants.

The HCHO formation rate equation at low DME pressures indicates that kinetic isotope effects reflect the ratio of rate constants given by

$$\mathrm{KIE}_{\mathrm{HCHO}} = \frac{k_{\mathrm{eff,1,H}}}{k_{\mathrm{eff,1,D}}} = \frac{K_{1,\mathrm{H}}k_{2,\mathrm{H}}}{K_{1,\mathrm{D}}k_{2,\mathrm{D}}} \qquad (7)$$

No H−D kinetic isotope effects are expected for DME physisorption and only weak effects for DME dissociation (K_1 and k_2), because these steps do not involve C−H bond cleavage.

The lack of a detectable kinetic isotope effect rules out any kinetic effects of C−H bond activation steps on the overall reaction and confirms the alternate kinetic relevance of DME dissociation at low DME reactant pressures.

Reaction rates at high DME pressures are only weakly influenced by H−D substitution and predominately reflect the values of the rate constants for reoxidation of oxygen vacancies:

$$\mathrm{KIE}_{\mathrm{HCHO}} = \frac{k_{\mathrm{eff,2,H}}}{k_{\mathrm{eff,2,D}}} = \frac{k_{6,\mathrm{H}}}{k_{6,\mathrm{D}}} \tag{8}$$

No H−D kinetic isotope effects are expected for vacancy reoxidation (k_6) because this step also does not involve C−H bond cleavage.

3.4. Isotopic Evidence for the Involvement of Lattice Oxygen Atoms and for the Reversibility of Dimethyl ether Dissociation Steps. Reactions of $CH_3OCH_3-CD_3OCD_3-O_2$ reactant mixtures were initially used to probe the reversibility of DME dissociation (step 2), but mixed DME isotopomers formed on Al_2O_3 supports and even on quartz reactor walls via acid-catalyzed DME−methanol interconversions involving water molecules formed in oxidation steps. Thus, these experiments failed to probe the reversibility of catalytically relevant steps that cleave and re-form C−O bonds in dimethyl ether.

Instead, we have used reactions of $CH_3{}^{16}OCH_3-{}^{18}O_2$ mixtures on $Mo^{16}O_3/Al_2{}^{16}O_3$ to probe concurrently the reversibility of DME dissociation steps, as well as the involvement of lattice oxygen atoms in HCHO formation. Involvement by lattice oxygen atoms would lead to the initial formation of $HCH^{16}O$ until lattice ^{16}O atoms become ultimately depleted and replaced by ^{18}O from $^{18}O_2$ co-reactants. Also, the involvement of lattice oxygen atoms would lead to significant ^{18}O introduction into unreacted DME, as lattice ^{16}O is replaced by ^{18}O from $^{18}O_2$, if DME dissociation steps are reversible and quasi-equilibrated.

We address first the involvement of lattice oxygen, because it is required before experimental data can be used to probe the reversibility of DME dissociation steps. Figure 6 shows the total (or cumulative) formation turnovers normalized per Mo for HCHO and CH_3OH isotopomers containing either ^{16}O or ^{18}O isotopes and their respective mole fractions as functions of residence time in a recirculating reactor at 488 K. Initially, when few ^{18}O atoms have replaced the ^{16}O initially present in the MoO_3 lattice, HCHO and CH_3OH contain mostly ^{16}O, as expected if lattice oxygens contributed the second O atom required to form two oxygenates from each $CH_3{}^{16}OCH_3$ molecule. As lattice oxygen vacancies form during turnovers and become reoxidized by $^{18}O_2$, the ^{18}O content in HCHO approached the 50% level expected as DME dissociates to form two indistinguishable methoxide groups containing one lattice oxygen and one oxygen atom from DME. The greater ^{16}O abundance in CH_3OH relative to HCHO indicates that CH_3OH is also formed via hydration of $CH_3{}^{16}OCH_3$ reactants, possibly on Lewis sites prevalent on the fractional portions of exposed Al_2O_3 support surfaces and without direct contribution from lattice oxygen. The $CH_3{}^{16}OH$ isotopomer concentration reaches an upper limit of 50% if methanol arises only from methoxide and hydroxyl groups chemisorbed on the $Mo^{18}O_x$ lattice. The ending $CH_3{}^{16}OH$ isotopomer concentration of 75% indicates that some methanol must result from reversible acid-catalyzed DME hydration reactions on exposed Al_2O_3. This introduces some complexity into our attempt to use these data to determine the reversibility of DME dissociation steps.

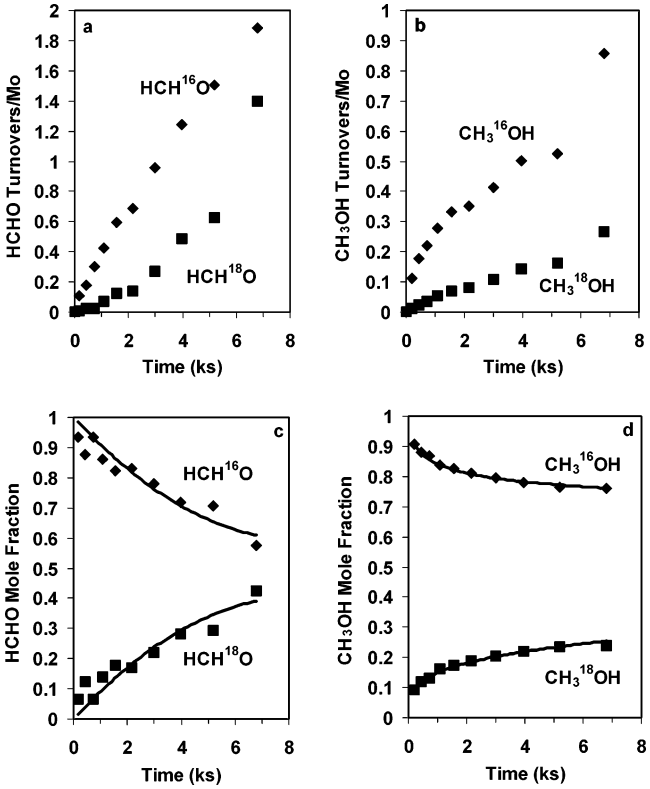

Figure 6. Cumulative (a) formaldehyde and (b) methanol isotopomer turnovers in $^{18}O_2-CH_3{}^{16}OCH_3$ mixtures on 15.6 wt % $Mo^{16}O_3/Al_2{}^{16}O_3$ (7 Mo/nm^2) and (c) formaldehyde and (d) methanol isotopomer distributions [13.6 kPa $CH_3{}^{16}OCH_3$, 20 kPa $^{18}O_2$, balance He, 488 K, gradientless batch reactor].

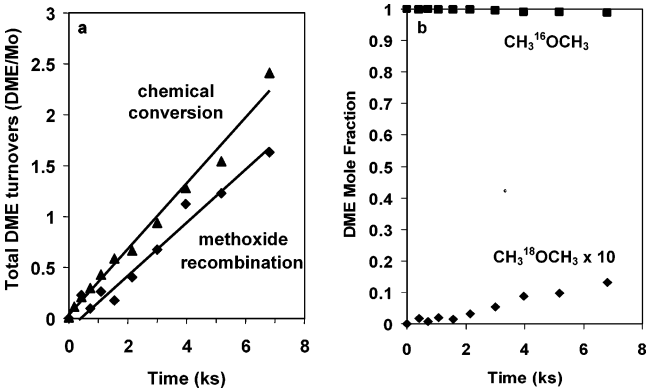

Figure 7. Total turnovers for DME chemical conversion and methoxy combination to re-form DME in $^{18}O_2-CH_3{}^{16}OCH_3$ (a) and DME isotopomer distribution (b) in mixtures on 15.6 wt % $Mo^{16}O_3/Al_2O_3$ (7 Mo/nm^2) [13.6 kPa $CH_3{}^{16}OCH_3$, 20 kPa $^{18}O_2$, balance He, 488 K, gradientless batch reactor].

Figure 7 shows total DME chemical conversion turnovers and methoxide recombination turnovers per Mo to form DME in the reverse of step 2. The latter were estimated as twice the number of $CH_3{}^{18}OCH_3$ formation turnovers, because after initial stages of the reaction, lattice oxygens are mostly ^{18}O and methoxide groups contain equal numbers of ^{16}O and ^{18}O atoms. The ratio of the rates of DME chemical conversion of reversible DME dissociation by methoxide recombination, as calculated from the slope of the graphs, is ∼1.3, suggesting that DME dissociation may be reversible, but not quasi-equilibrated, during DME oxidation to HCHO on this catalyst. Quasi-equilibration requires the rate of methoxide recombination to be considerably

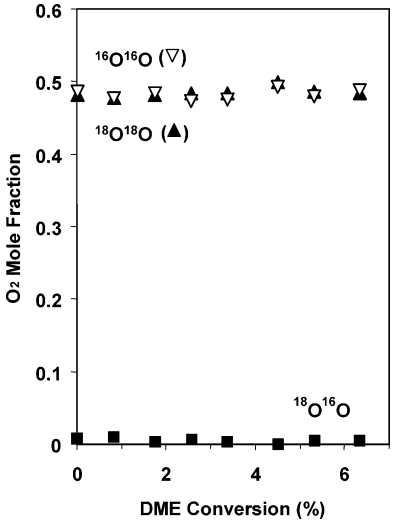

Figure 8. $^{18}O^{16}O$ mole fraction in O_2 reactant during the reaction of CH_3OCH_3 and a mixture of $^{16}O_2-^{18}O_2$ on 15.6 wt % MoO_3/Al_2O_3 (7 Mo/nm^2) [17 kPa DME, 2.4 kPa $^{16}O_2$, 2.4 kPa $^{18}O_2$, balance He, 513 K, gradientless batch reactor].

larger than that of chemical reaction and it would have led to similar ^{18}O contents in DME reactants and in all reaction products. Figure 7b shows that this is not the case. This rate of ^{18}O introduction into DME is, in fact, an upper limit for the rate of the reverse of step 2, because the reversible reaction of $CH_3{}^{16}OCH_3$ with $H_2{}^{18}O$ formed during HCHO synthesis via hydration reactions occurs and leads to ^{18}O introduction into "unreacted" DME. Thus, our assumption that step 2 is essentially irreversible in deriving kinetic rate equations consistent with experimental data appears to be justified.

The irreversible nature of O_2 dissociative chemisorption steps on surface vacancies (step 6) was examined by measuring the dioxygen isotopomers formed during reactions of $CH_3{}^{16}OCH_3$ with equimolar $^{16}O_2-^{18}O_2$ mixtures. Quasi-equilibrium would lead to binomial dioxygen isotopomers (50% $^{16}O^{18}O$), while irreversible dissociation steps would preserve the isotopic identity of the O_2 in the reactant mixture, even as chemical conversion increases. Figure 8 shows the oxygen isotopomer distribution as a function of DME conversion in a recirculating batch reactor. No mixed dioxygen isotopomers were detected at any chemical conversion levels (0−5%). Thus, dioxygen dissociation steps are irreversible during catalytic DME oxidation on MoO_3/Al_2O_3. This conclusion is consistent with the stability of MoO_3 against autoreduction in inert or oxygen-containing environments at typical DME oxidation temperatures and with the role and irreversibility of O_2 dissociation steps in other oxidation reactions, such as the oxidative dehydrogenation of alkanes on supported MoO_x, VO_x, and WO_x domains.[29,32,33]

3.5. Comparison for Methanol and DME Oxidation Kinetics and Catalyst Requirements. DME molecules form two methoxide molecules during each dissociation step, while each CH_3OH forms only one, yet DME converts to HCHO more slowly than CH_3OH. Methanol oxidation to HCHO occurs via quasi-equilibrated dissociation of O−H bonds to form adsorbed methoxide followed by kinetically relevant C−H bond activation of surface methoxide using lattice oxygen atoms.[31] First-order HCHO synthesis turnover rates are about 10 times larger for CH_3OH than for DME reactants at 493 K (1.83×10^{-3} vs 1.94×10^{-4} s^{-1}), because the C−O dissociation steps required to form methoxide precede C−H bond activation steps, which limit rates for DME oxidation reactions.

CH_3OH and DME oxidation rates both depend on the identity of the support used to disperse active oxide domains.[8,9,34−37] CH_3OH oxidation rates on supported polymolybdate monolayers varied by more than a factor of 10 on various supports and rates increased with decreasing electronegativity of support cations ($ZrO_2 \sim TiO_2 \gg Nb_2O_5 > Al_2O_3 > SiO_2$).[36,37] Support effects on supported vanadia catalysts are even stronger, and rates varied by 3 orders of magnitude as a function of support identity.[34] Rates for DME oxidation and for stoichiometric reduction of MoO_3 domains with H_2 increased in parallel with changes in the support used to dispersed MoO_3 domains ($SnO_2 > ZrO_2 > Al_2O_3 > MgO$), suggesting that the reactivity of active oxide domains depends sensitively on their ability to delocalize electron density during rate-determining steps.[9] Turnover rates increased with increasing reducibility of Mo centers, which were influenced in turn by the size of the MoO_3 domains and by the identity of the support materials. Similar effects were reported earlier for alkane oxidative dehydrogenation, for which kinetically relevant C−H bond activation steps required reduction of metal centers during each catalytic turnover.[38] A similar argument seems plausible for methanol oxidation, which occurs via rate-determining C−H bond activation steps, normally associated with the formal reduction of metal centers. Support effects were substantiated when Oyama et al.[39] showed that the activity of a catalyst correlates with the density of unoccupied electronic states; MoO_x deposited on support materials that readily accept electron density from reducing C−H bond cleavage steps in methanol oxidation result in higher conversion rates.[39]

This reasoning becomes less unequivocal for the observed correlations between reducibility and DME oxidation rates, because H-abstraction appears to be kinetically irrelevant and C−O bond cleavage, which limits reaction rates, does not require the formal reduction of Mo^{6+} centers. It appears, however, that electron density at cation sites increases gradually along the reaction sequence, instead of occurring sharply during the formal reduction assumed to occur at the H-abstraction step. The formation of methoxide species, via either O−H dissociation in CH_3OH or C−O cleavage in DME, appears to require electron transfer, which is most effectively accommodated by reducible cations. Activated complexes involved in forming methoxide intermediates become stabilized by effective electron delocalization and activation energies consequently decrease. This charge delocalization is imposed by the required cleavage of a bridging metal−oxygen bond, which is replaced by one bond from each metal atom to a methoxide species, a process that leads to charge delocalization of the metal centers due to the different extent of charge separation in M−O−M and M−O−CH_3.

These arguments find qualitative support in previous studies of methanol reactions, which found that equilibrium constants for CH_3OH adsorption as methoxides increased 6-fold and rate constants for H-abstraction from methoxide increased ~20-fold with changes in the support used to dispersed polyvanadate monolayers ($CeO_2 > ZrO_2 > TiO_2 > Al_2O_3$).[23] These supports have also been reported to influence in a similar sequence the reducibility of MoO_x and VO_x monolayers,[8,9] because of their apparent ability to delocalize charge away from the active oxide domains during redox cycles. Similarly, such arguments can rationalize the support effects on our DME oxidation rates over dispersed molybdate domains as DME dissociation is not unlike CH_3OH dissociation; neither step requires formal reduction of metal centers.

4. Conclusions

In situ infrared spectroscopy at low DME pressures indicated that methoxides are chemisorbed on the MoO_x surface during DME oxidation reactions and that they are intermediates to HCHO and CH_3OH. Kinetic studies by varying DME and O_2 pressures led to HCHO and CH_3OH formation rates that were first-order in DME and zero-order in O_2 at low DME pressure. These rates approach zero-order in DME and are positive-order in O_2 at high DME pressure as lattice oxygen vacancies become abundant. Under these conditions, surface hydroxyl groups formed by methoxide C−H activation combine mainly with methoxide to form CH_3OH (instead of with another hydroxyl group to form water) leading to equimolar HCHO and CH_3OH formation. H−D kinetic isotope effects indicated that C−H bond activation of surface methoxide is not a kinetically relevant step and transient reactions with $CH_3{}^{16}OCH_3-{}^{18}O_2$ mixtures demonstrated the kinetic relevance of DME dissociative adsorption at low DME pressure. This step precedes C−H bond activation and was found to be nearly irreversible. Reactions with $^{18}O_2$-$^{16}O_2$ did not produce detectable amounts of $^{16}O-{}^{18}O$; the reoxidation of lattice oxygen vacancies was found to be irreversible.

A reaction mechanism was proposed for DME oxidation and the kinetic rate equations derived from the mechanism were shown to be consistent with spectroscopic studies and with observed dependencies on reactant pressures and with isotopic studies.

Acknowledgment. This study was supported by BP as part of the Methane Conversion Cooperative Research Program at the University of California at Berkeley.

Appendix

Since M−O bonds are broken and formed concurrently, M* and O* exist in equal amounts.

$$[M^*] = [O^*]$$

At low P_{DME} pressure, the surface is uncovered and oxidized and no methanol is formed. The derivation for HCHO formation rate is as follows:

$$\frac{d[^*OCH_3]}{dt} = 2K_1k_2\frac{[M^*][O^*]}{C_t}P_{DME} - 2k_3\frac{[^*OCH_3][O^*]}{C_t} = 0$$

$$[^*OCH_3] = \frac{K_1k_2}{k_3}[M^*]P_{DME} = \frac{K_1k_2}{k_3}[O^*]P_{DME}$$

$$C_t = [M^*] + [O^*] = 2[O^*]$$

$$[O^*] = \frac{C_t}{2}$$

$$r_{HCHO} = k_3\frac{[^*OCH_3][O^*]}{C_t} = K_1k_2\frac{[M^*][O^*]}{C_t}P_{DME}$$

$$r_{HCHO} = \frac{1}{4}K_1k_2P_{DME}$$

At high P_{DME} pressure, the rates of HCHO and CH_3OH formation are equal. The rate of HCHO formation can be derived as

$$\alpha = 1 = \frac{r_{CH_3OH}}{r_{HCHO}} = \frac{k_4[^*OCH_3][OH^*]}{k_3[^*OCH_3][O^*]}$$

$$[^*OH] = \frac{k_3}{k_4}[O^*]$$

$$[^*OCH_3] = \frac{K_1k_2}{k_3}[O^*]P_{DME}$$

$$\frac{d[^*]}{dt} = 2k_3\frac{[^*OCH_3][O^*]}{C_t} - k_6\frac{[^*]^2}{C_t}P_{O_2} = 0$$

$$[^*] = \left(\frac{2K_1k_2}{k_6}\frac{P_{DME}}{P_{O_2}}\right)^{1/2}[O^*]$$

$$C_t = [M^*] + [O^*] + [^*OCH_3] + [^*OH] + [^*]$$

$$[O^*] = \frac{C_t}{2 + \frac{K_1k_2}{k_3}P_{DME} + \frac{k_3}{k_4} + \left(\frac{2K_1k_2}{k_6}\frac{P_{DME}}{P_{O_2}}\right)^{1/2}}$$

$$r_{HCHO} = \frac{K_1k_2}{\left\{2 + \frac{K_1k_2}{k_3}P_{DME} + \frac{k_3}{k_4} + \left(\frac{2K_1k_2}{k_6}\frac{P_{DME}}{P_{O_2}}\right)^{1/2}\right\}^2}P_{DME}$$

At large P_{DME}/P_{O_2} ratios, lattice oxygen vacancies become the most abundant reactive intermediate. The HCHO formation rate becomes

$$r_{HCHO} = \frac{1}{2}k_6P_{O_2}$$

References and Notes

(1) Brown, S. H.; Green, L. A.; Mathias, M. F.; Olson, D. H.; Ware, R. A.; Weber, W. A.; Shinnar, R. U.S. Patent 6,506,954, 2003.
(2) Brown, S. H.; Green, L. A.; Mathias, M. F.; Olson, D. H.; Ware, R. A.; Weber, W. A. U.S. Patent 6,046,372, 2000.
(3) Brown, S. H.; Shinnar, R.; Weber, W. A. U.S. Patent 6,613,951, 2003.
(4) Brown, S. H.; Weber, W. A.; Shinnar, R.; Nariman, K. E.; Green, L. A.; Mathias, M. F.; Olson, D. H.; Ware, R. A. U.S. Patent 6,538,167, 2003.
(5) Barger, P. T. U.S. Patent 5,248,647, 1991.
(6) Fleisch, T. H.; Basu, A.; Gradassi, M. J.; Masin, J. G. *Stud. Surf. Sci. Catal.* **1997**, *107*, 117.
(7) Li, J. L.; Zhang, X. G.; Inui, T. *Appl. Catal., A: Gen.* **1996**, *147*, 23.
(8) Liu, H. C.; Cheung, P.; Iglesia, E. *Phys. Chem. Chem. Phys.* **2003**, *5*, 3795.
(9) Liu, H. C.; Cheung, P.; Iglesia, E. *J. Catal.* **2003**, *217*, 222.
(10) Liu, H. C.; Cheung, P.; Iglesia, E. *J. Phys. Chem. B* **2003**, *107*, 4118.
(11) Liu, H. C.; Iglesia, E. *J. Catal.* **2002**, *208*, 1.
(12) Lewis, R. M.; Ryan, R. C.; Slaugh, L. H. U.S. Patent 4,442,307, 1984.
(13) Lewis, R. M.; Ryan, R. C.; Slaugh, L. H. U.S. Patent 4,439,624, 1984.
(14) Lewis, R. M.; Slaugh, L. H. U.S. Patent 4,435,602, 1984.
(15) Chen, K. D.; Xie, S.; Bell, A. T.; Iglesia, E. *J. Catal.* **2001**, *198*, 232.
(16) Iglesia, E.; Baumgartner, J. E.; Price, G. L. *J. Catal.* **1992**, *134*, 549.
(17) Price, G. L.; Iglesia, E. *Ind. Eng. Chem. Res.* **1989**, *28*, 839.
(18) Briand, L. E.; Farneth, W. E.; Wachs, I. E. *Catal. Today* **2000**, *62*, 219.
(19) Burcham, L. J.; Briand, L. E.; Wachs, I. E. *Langmuir* **2001**, *17*, 6175.
(20) Campbell, S. M.; Jiang, X. Z.; Howe, R. F. *Microporous Mesoporous Mater.* **1999**, *29*, 91.
(21) Chung, J. S.; Miranda, R.; Bennett, C. O. *J. Chem. Soc. Faraday Trans. 1* **1985**, *81*, 19.
(22) Narishige, N.; Niwa, M. *Catal. Lett.* **2001**, *71*, 63.
(23) Burcham, L. J.; Wachs, I. E. *Catal. Today* **1999**, *49*, 467.

(24) Seman, M.; Kondo, J. N.; Domen, K.; Radhakrishnan, R.; Oyama, S. T. *J. Phys. Chem. B* **2002**, *106*, 12965.
(25) Groff, R. P. *J. Catal.* **1984**, *86*, 215.
(26) Mars, P.; Van Krevelen, D. W. *Chem. Eng. Sci. Spec. Suppl.* **1954**, *3*, 41.
(27) Pernicone, N.; Lazzerin, F.; Liberti, G.; Lanzavecchia, G. *J. Catal.* **1969**, *14*, 293.
(28) Chen, K. D.; Iglesia, E.; Bell, A. T. *J. Phys. Chem. B* **2001**, *105*, 646.
(29) Chen, K. D.; Khodakov, A.; Yang, J.; Bell, A. T.; Iglesia, E. *J. Catal.* **1999**, *186*, 325.
(30) Argyle, M. D.; Chen, K.; Bell, A. T.; Iglesia, E. *J. Phys. Chem. B* **2002**, *106*, 5421.
(31) Machiels, C. J.; Sleight, A. W. *J. Catal.* **1982**, *76*, 238.
(32) Chen, K. D.; Bell, A. T.; Iglesia, E. *J. Phys. Chem. B* **2000**, *104*, 10059.
(33) Chen, K. D.; Iglesia, E.; Bell, A. T. *J. Catal.* **2000**, *192*, 197.
(34) Deo, G.; Wachs, I. E. *J. Catal.* **1994**, *146*, 323.
(35) Wachs, I. E. In *Catalysis*; Spivey, J. J., Ed.; The Royal Society of Chemistry: Cambridge, U.K., 1997; Vol. 13; p 37.
(36) Burcham, L. J.; Badlani, M.; Wachs, I. E. *J. Catal.* **2001**, *203*, 104.
(37) Hu, H.; Wachs, I. E. *J. Phys. Chem.* **1995**, *99*, 10911.
(38) Chen, K. D.; Bell, A. T.; Iglesia, E. *J. Catal.* **2002**, *209*, 35.
(39) Oyama, S. T.; Radhakrishnan, R.; Seman, M.; Kondo, J. N.; Domen, K.; Asakura, K. *J. Phys. Chem. B* **2003**, *107*, 1845.